5 MECHANICALLY TUNABLE THIN FILMS OF PHOTOSENSITIVE ARTIFICIAL PROTEINS CHARACTERIZED BY AFM NANOINDENTATION

5.1 Abstract

Thin films with tunable stiffness were made by photocrosslinking an artificial extracellular matrix protein that was biosynthesized to contain *para*-azidophenylalanine (*p*N_3Phe). The elastic moduli of the films were calculated from nanoindentation data collected by atomic force microscopy (AFM) using a thin-film Hertz model. Film elastic modulus was shown to be tunable in the range of 0.3 to 1.0 MPa either by differential irradiation or by varying the level of *p*N_3Phe in the protein. Tensile measurements on bulk films of the same proteins and finite-element simulation of the indentation agreed with the thin-film modulus calculations. Single substrates with patterns of mechanical properties were created; these have potential use in studying mechanically dependent cell behavior, particularly in the context of coordinating biological signals.

Manuscript prepared for submission by Paul J. Nowatzki[1], Christian Franck[2], Guruswami Ravichandran[2], and David A. Tirrell[1].

(1) Division of Chemistry and Chemical Engineering, California Institute of Technology

(2) Graduate Aeronautics Laboratories, California Institute of Technology

5.2 Introduction

5.2.1 Mechanical sensitivity of cell behavior.

Although cells are known to respond to chemical signals, the mechanical properties of their environment are increasingly being recognized as an additional important determinant of cell behavior. Differences in substrate stiffness have been shown to affect cell adhesion,[1,2] spread area and shape,[1,3,4] traction forces and migration rate,[1,5,6] growth,[7] and differentiation.[2,8] Mechanical effects are thus postulated to play an important role in aspects of biology ranging from cell morphology to embryonic development.[9]

Cell-culture substrates with adjustable mechanical properties are essential tools for studying these phenomena. Stiffness-dependent cell behavior reported to date has most frequently been characterized on chemically crosslinked synthetic gels such as polyacrylamide.[1,5,10] Because biological and mechanical signals are expected to have coordinating effects,[9,11] in some cases it will be preferable to study cells on substrates that more closely mimic the extracellular matrix; for example, collagen-coated gels have been used.[3,8] The ability to vary mechanical properties on a single substrate would be useful in probing many conditions at once and reducing experimental variability. Moreover, films with stiffness patterns can elucidate cell behavior at mechanical interfaces,[5] and stiffness gradients allow research into what is termed mechanotaxis or durotaxis.[6,12,13]

5.2.2 Artificial protein.

We use a photosensitive artificial protein to make substrates in which the coordinating effects of stiffness and extracellular matrix biology can be studied directly. It is based on a family of previously reported artificial proteins intended for use as implantable biomaterials, which were designed to mimic key features of the extracellular matrix.[14-17] The design contains cell binding domains periodically spaced between elastin-like repeating peptides that confer flexibility; the amino acid sequence is shown in Figure 5.1. The CS5 cell binding domain, taken from the alternatively spliced type III connecting segment region of human fibronectin, serves as a means of attaching cells that express the $\alpha_4\beta_1$ integrin cell surface receptor.[18] The basis for the elasticity of the artificial protein is the repeating peptide VPGVG (Val-Pro-Gly-Val-Gly), derived from mammalian elastin and known to reproduce many of its properties.[19]

MMASMTGGQQMGRKTHHHHHHMG-
{LDGEEIQIGHIPREDVDYHLYPG[(VPGVG)$_2$(VPG**F**G)(VPGVG)$_2$]$_5$LP}$_3$LE

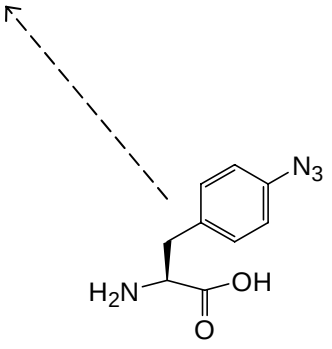

pN$_3$Phe

Figure 5.1 Amino acid sequence of the artificial extracellular matrix protein. The cell-binding sequence CS5 is underlined. The fifteen phenylalanines, **F**, are partially replaced by *para*-azidophenylalanine (right) in synthesis; protein containing this photosensitive amino acid is designated aE-*p*N$_3$Phe. In the notation aE-n%-*p*N$_3$Phe, n% indicates the fraction of Phe that is replaced with *p*N$_3$Phe.

The phenylalanine (Phe) sites dispersed throughout the elastin-like portion serve as sites for the incorporation of the non-canonical amino acid *para*-azidophenylalanine (*p*N_3Phe, Figure 5.1), which is accomplished by using a bacterial clone that expresses a mutant phenylalanyl-tRNA synthetase (PheRS) with an enlarged binding pocket.[20,21] The azide group of *p*N_3Phe is UV-photolysable, generating a nitrene that yields non-specific crosslinks to surrounding protein molecules. By varying the concentration of *p*N_3Phe during bacterial synthesis, the level of substitution for Phe in the protein can be tuned, thereby altering the crosslink density and elastic modulus of UV-irradiated protein films.[22] The photocrosslinking technique has already been used with a photomask to selectively pattern protein on substrates, demonstrating that a cell-adhesive protein can be presented to cells in predetermined geometries.[22] Herein we report the creation and characterization of thin films of this protein; their elastic moduli are tunable by variable *p*N_3Phe incorporation, in parallel to results on bulk films. Furthermore, variable irradiation of a protein with high *p*N_3Phe content allowed patterns (step-gradients) of mechanical properties to be made on a single film.

5.2.3 AFM characterization.

Mechanical properties of thin, substrate-bound films are typically measured by nanoindentation, and atomic force microscopy (AFM)-based nanoindentation in particular offers significant advantages in spatial and force resolution over conventional nanoindenters. It is therefore appropriate for

analyzing soft samples and materials whose stiffness varies on short length scales.[23-25] Here, AFM nanoindentation with a microspherical tip (600 nm diameter) was used to obtain accurate measurements of film elastic modulus.[26,27] The use of a spherical tip allows a spherical indentation model to be correctly applied, since the classical Hertz spherical model is known to cause distortions when used to analyze AFM data collected with conventional sharp, pyramidal or conical tips.[28] A film-height dependent physical model[29] accounts for the mechanical coupling of the film to its underlying support, another known source of distortion in AFM nanoindentation.[30,31] Bulk tensile tests of the same materials confirm the nanoindentation calculations made with this model.

Finite element simulations of the indentations were also performed to verify the modulus calculations and to explore the possibility of determining a more sophisticated mechanical material model from AFM data. While the linear elasticity model[29] accurately measures initial elastic modulus of the films described herein, the finite element analysis will be appropriate for characterizations of thinner films, higher strain indentation data, and arbitrary tip geometry.

5.3 Experimental

*5.3.1 Protein aE-*p*N*$_3$*Phe.*

The amino acid sequence of the photosensitive artificial extracellular protein, aE-*p*N$_3$Phe, is shown in Figure 5.1. It is made biosynthetically in a Phe-

auxotrophic strain of *E. coli* with a plasmid bearing genes coding for both the protein and the Ala294Gly mutant of the *E. coli* phenylalanyl-tRNA synthetase (PheRS),[32] which allows incorporation of *p*N_3Phe (Bachem) in place of Phe when the protein expression is induced.[21]

The expression and purification of the protein, designated aE-*p*N_3Phe, were based on previous work.[22] To ensure that Phe was depleted from the medium during protein synthesis, the cells were centrifuged and resuspended in minimal medium lacking Phe and containing *p*N_3Phe 10 minutes after expression was induced, enough time for functional copies of the PheRS to be synthesized.

The incorporation level of *p*N_3Phe was measured by 600 MHz ^{1}H NMR (Varian) at a protein concentration of 15 mg/mL in DMSO-d_6 (Cambridge Isotope Laboratories) by comparing the distinct aromatic proton peak areas assigned to *p*N_3Phe and to Phe.[22] Phe replacement levels of 28%, 31%, 48%, and 66% were achieved by using 125, 188, 250, and 250 mg/L, respectively, of *p*N_3Phe in the culture medium; the corresponding proteins are designated aE-28%-*p*N_3Phe, etc.

5.3.2 AFM – equipment.

Images and force curves were collected on a Park Scientific Instruments AutoProbe M5 atomic force microscope, with accompanying ProScan v1.51b software. Pyramidal-tipped triangular silicon nitride cantilevers with nominal spring constant 0.58 N/m were used for imaging (Veeco DNP-S). A silicon nitride cantilever of the same shape, with an attached 600 nm diameter SiO_2 particle tip (Novascan, Ames, IA), was used to indent samples for collecting force

curves. Its spring constant was calculated to be 0.37 N/m by indenting against reference cantilevers with predetermined spring constants of 1.00 N/m and 0.125 N/m (Veeco CLFC). Here, $k_{test}/k_{ref} = (\delta_{tot} - \delta_{test})/(\delta_{test} \cos\theta)$, where k_{test} and k_{ref} are the spring constants of the test and reference cantilevers, δ_{tot} and δ_{test} are slopes of the force-distance curve when the test cantilever is indented against a rigid surface and the free end of the reference cantilever, and θ is the angle between the cantilevers (15°). A glass slide was glued to the back of the cantilever mount so that the cantilever and sample could be submerged in water.

5.3.3 Bulk protein films.

aE-*p*N_3Phe (4 mg) was dissolved in dimethylsulfoxide (40 μL, Mallinckrodt). The solution was spread to cover an area approximately ~1.5 cm × 1 cm on a poly(methyl methacrylate) surface, and the solvent was evaporated at 50 °C overnight. The resulting films were ~20 μm thick (dry). Once irradiated (*vide infra*), uniaxial tension tests were performed on the samples at 22 °C using an Instron 5542 with 0.5 N load cell, modified to contain the sample in a water bath; strain rate was 10% of the original length per minute,[33] at which viscoelastic effects are negligible.

5.3.4 Thin protein films.

All film-making procedures were performed in a cold room (4 °C), below the lower critical solution temperature (LCST)[19] of the protein in water. Protein (10 mg) was dissolved in water (100 μL), and the solution was centrifuged (5 min,

16,500×*g*) to remove any aggregates or particles. Protein solution (10 μL) was pipetted onto and spread to cover an unmodified 12 mm glass slide (Hecht-Assistent, Sondheim, Germany). Films were spin-coated (Specialty Coating Systems, Inc. P6204, Indianapolis, IN) at 7,000 rpm for 30 seconds and dried overnight at 4 °C. Typical film thickness was ~200 nm (dry).

5.3.5 Irradiation of films.

Dry protein films were exposed to unfiltered UV light from a high-pressure mercury arc lamp (Oriel Q, 100 watt @ 5 amps, > 20 min warm-up time; measured intensity in irradiation plane = 1.5 mW/mm^2). Time to achieve complete conversion, ~300 sec, was determined empirically. Zones of differential crosslinking were achieved on the same substrate by placing an opaque shutter over portions of the film during irradiation. Specifically, a step-gradient of irradiation times (0, 12, 20, 30, 50, 80, 120, 180, and 300 sec) was made across a 12 mm slide by manually repositioning the shutter between exposures.

Slides were agitated in excess water, 4 °C, to remove any soluble protein. Un-irradiated protein, or protein irradiated for 12 sec or less, was completely removed during this rinsing process as evidenced by AFM imaging. No delamination of irradiated films from their glass substrates was observed.

5.3.6 AFM – film thickness.

The tip of a pair of fine forceps was lightly dragged across the surface of the protein film, tearing away the protein along the scratch and revealing the

underlying glass substrate. The edge of this scratch was imaged by AFM both dry and under water; the thickness of the film is apparent from the scan (see Figure 5.2). The surface revealed by the scratch was confirmed to be glass, based on its smoothness and linear force profile when indented. The protein film thickness was calculated by averaging the height measurements at many ($n \geq 16$) points on the film, using the revealed glass surface as a baseline.

5.3.7 AFM – indentation force curves.

The films and cantilever assembly were submerged in water under ambient conditions. The 600-nm SiO_2 microsphere tip was placed above a spot where the film thickness had been measured (identified visually from the optical microscope image using reference markers on the film) to ensure that the thickness at the point of indentation was known. Force curves were collected; the instrument records z (piezo) displacement and force, the product of measured tip deflection and cantilever spring constant.

The indentation range was set to (-150 nm, +1350 nm) relative to the contact point, effectively limiting the force to ~20-30 nN and the strain magnitude to under 20%. The indent-retract cycle time was 1 sec (tip speed 3 μm/sec). Viscoelastic effects did not appear to be a significant factor at this strain rate (~4 sec^{-1}), as evidenced by the statistical superimposability of force curves collected using 1 sec and 10 sec cycles (~0.4 sec^{-1}), Figure 5.4.

To assess the uniformity of the mechanical properties, force curves were evaluated repeatedly at the same spot and at nearby spots spaced 10-20 μm

apart. For the uniformly-irradiated *p*N$_3$Phe films this procedure was repeated at three distant (> 1 mm apart) spots of individually-measured height.

5.3.8 Calculation of elastic modulus.

The Dimitriadis model[29] for indentation of linear-elastic soft material films of finite height with a spherical indenter was applied to the loading force data. For a support-bonded film of Poisson ratio $\nu = 0.5$ (incompressible, a reasonable estimate for both for rubbery networks and biological materials):

$$F = \frac{16E}{9} R^{1/2} \delta^{3/2} [1 + 1.133\chi + 1.283\chi^2 + 0.769\chi^3 + 0.0975\chi^4] \quad (1)$$

The first term of this series is the classical Hertz indentation model of force F as a function of (Young's) elastic modulus E and indentation depth δ using a rigid sphere of radius R. Additional terms were added[29] to correct for the finite height of the film, where χ is given by:

$$\chi = \sqrt{R\delta} / h \quad (2)$$

and h is the thickness of the film. As the film gets thinner, or as the indentation depth increases, the indenting sphere (AFM tip) experiences a higher force than it would for an infinitely-thick film of the same material, owing to mechanical effects of film confinement to the stiff underlying substrate. The film indentation δ was calculated by subtracting the tip displacement from the total (z) displacement.

The contact point of the force-distance curves, where the indentation and force were set to zero in the analysis, was determined by visual inspection.

While this can be difficult in some experiments,[29] it is straightforward for the force curves collected here, because we observe a distinct snap-in when the tip touches the surface (see Figure 5.3 for examples). The apparent elastic modulus was calculated by evaluating equations (1) and (2) at each recorded force-indentation point between 15 nm and 10% film indentation and averaging over the range. Below 15 nm, the scatter in the data is magnified in the calculations and distortions are common; the 10% maximum indentation is to constrain the data to the near-linear response range.[29] In this strain range, the finite-height correction factor was as large as 1.78 ($\chi = 0.395$) for the films analyzed here.

5.3.9 Finite element simulation.

A simulation of the indentation was constructed in the program ABAQUS (ABAQUS, Inc., Providence, RI). The system was represented by 2D axisymmetric elements (CAX4R) using the known protein film height and indenting tip geometry (R = 300 nm). From tensile data collected for bulk samples of aE-*p*N_3Phe, material model parameters for each material were calculated and entered into the simulation. The Yeoh model[34] was found to best describe the material response of aE-*p*N3Phe as determined through numerous uniaxial tension and compression tests. The output of force versus film indentation was compared to the AFM data collected experimentally.

5.4 Results and Discussion

5.4.1 Thin films.

The spin-coated thin films of aECM protein appeared smooth (RMS roughness = 1.3 nm, versus 0.9 nm for the revealed glass) when imaged by AFM, Figure 5.2. The film thickness was uniform over the surface of a given 12 mm glass slide substrate, varying no more than ± 10% from the average. The local thickness was much more uniform, with < 2% variation in a 30 μm scan. The hydrated thicknesses of the protein films ranged from 191 to 418 nm. Two thicker films, made using a higher concentration of aE-66%-*p*N_3Phe, were ~1500 nm thick (Table 5.1).

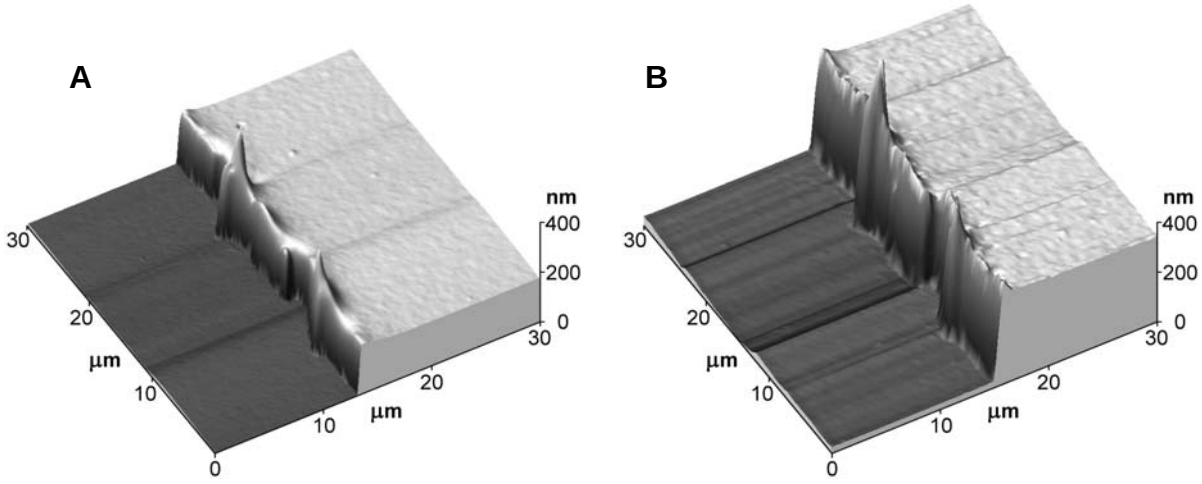

Figure 5.2 AFM topography scans of an aE-48%-*p*N_3Phe film, dry (A) and in water (B). The z scales (height) are exaggerated 22× relative to the x and y scales. The film (right side of images) was scratched to reveal the underlying glass substrate (left), indicating the height of the film; the spikes at the edge are artifacts of the scratching procedure. This film was 178 nm thick dry and 328 nm thick wet.

5.4.2 AFM force curves.

Representative loading force curves are shown in Figure 5.3; these display the parabolic shape typical of soft materials. Since the assembly is submerged in water, the attractive force between the tip and the surface is screened; nevertheless, a distinct snap-in is seen for each force curve, which allows a contact point to be confidently assigned. In cases where the snap-in appeared to occur over a few nanometers, the contact point was assigned to the middle of the snap-in rather than the bottom (at minimum force), as this was found to give the best reproducibility between repeated indentations at the same spot.

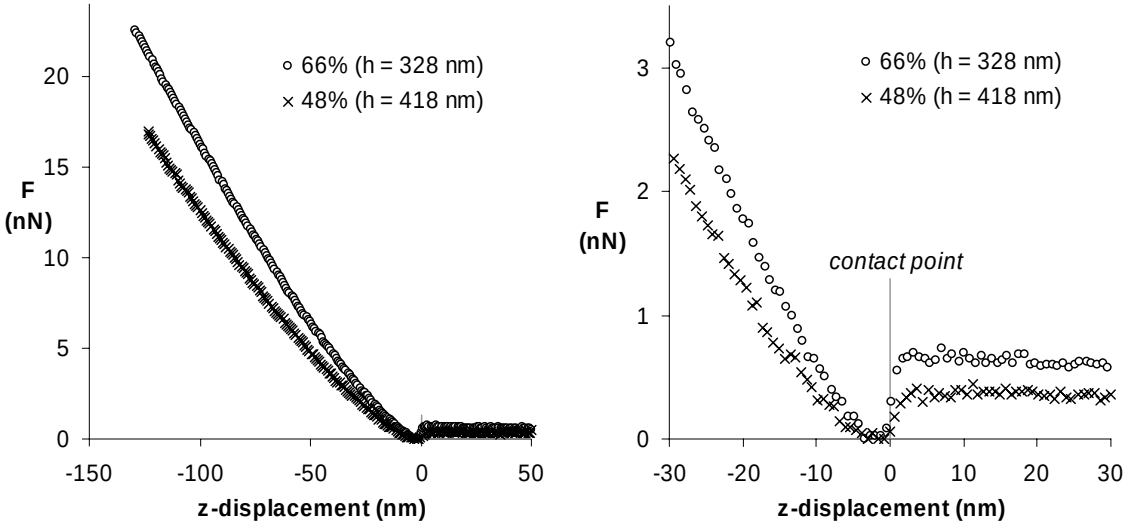

Figure 5.3 Representative loading indentation profiles for thin protein films of aE-66%-*p*N$_3$Phe and aE-48%-*p*N$_3$Phe, showing force versus z-displacement (equal to cantilever deflection plus film indentation). The raw force and displacement data have been zeroed using the snap-in to establish the contact point. The figure on the right is magnified to show the contact point assignment.

When the strain rate was reduced by a factor of 10 from the experimental rate (1 sec indent cycle, ~4 sec^{-1}), the resulting force curves appeared indistinguishable from the originals, an indication that viscoelastic effects did not significantly influence the results (Figure 5.4). Faster indentation cycles allow increased throughput and minimize the deleterious effects of sensor drift.

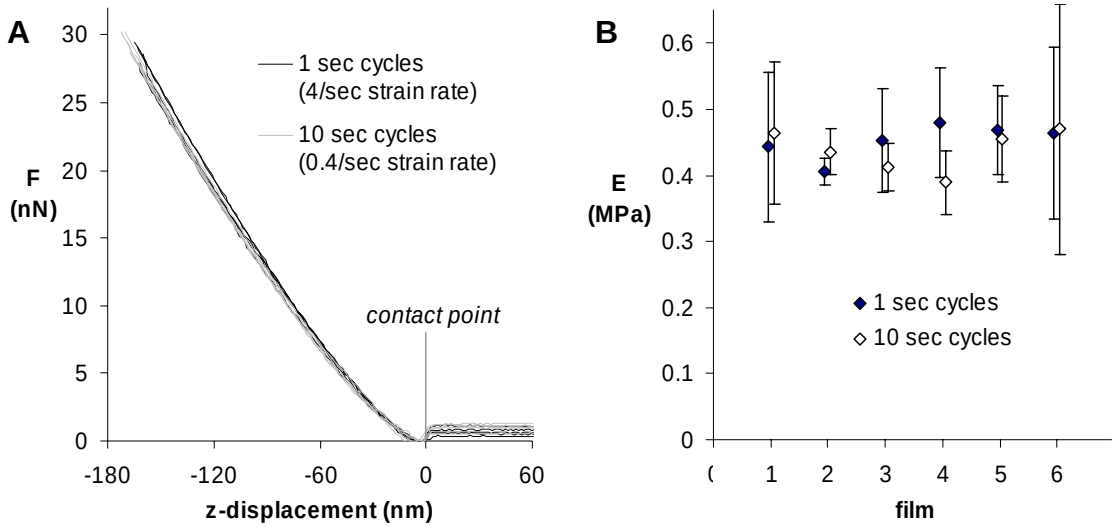

Figure 5.4 (A) Superimposed force profiles for multiple indentations (n=5) of a single aE-48%-*p*N_3Phe film using 1 sec (used herein) and 10 sec indent cycles. (B) Elastic moduli, E, calculated (see 5.4.3) using 1 sec and 10 sec indent cycles on five different aE-48%-*p*N_3Phe films (h = 217-293 nm, n≥4). No significant differences are seen based on cycle time. 1 sec indent cycles (~4 sec^{-1} strain rate) were used for all modulus data reported in this work.

Repeated indentations (up to 100) of the same spot did not cause any change in the force curves, likely because the hydrated protein films are highly elastic and the indentation depth was controlled. When surfaces on which the indentations had been performed were subsequently imaged by AFM, no

evidence of indentation was seen on either hydrated or dry films. This supports the conclusion that the collection of force curves here does not permanently deform or otherwise alter the mechanical properties of the samples.

5.4.3 Analysis of AFM force curves.

Once a force curve is collected, all variables in the equations (1) and (2) except E are known, so each point on the force-distance curve can be used to calculate an elastic modulus for the material. If the model describes the system correctly, the calculated modulus should be the same at each indentation depth. The Hertz and Dimitriadis[29] models were evaluated using this criterion for a representative data set in Figure 5.5. Because the films were less than a micron in thickness and the indentation depth represented a significant portion of the film height, the infinite-height Hertz model was inappropriate for elastic modulus calculation. The elastic properties of the protein films were significantly influenced by the underlying glass substrate, as has been observed previously for soft thin films.[29,30] Because it accounted for the finite sample thickness and coupling to a rigid substrate, the Dimitriadis model was much more effective, resulting in consistent predictions of modulus for each force curve in the indentation range of 15 nm to 10% or more of the film thickness.

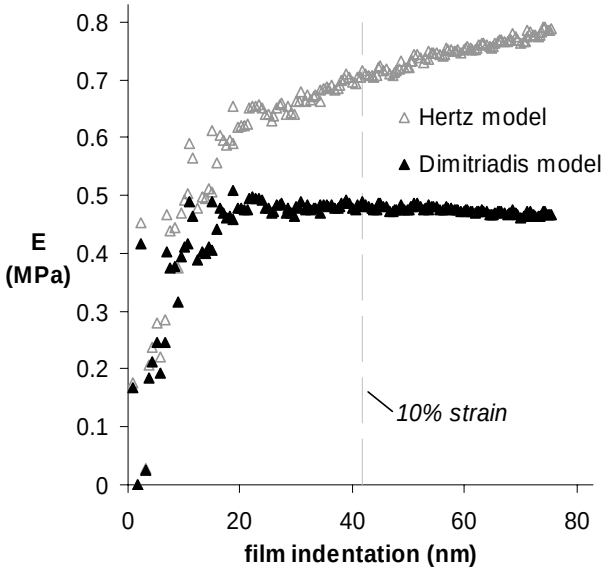

Figure 5.5 The elastic modulus (E) calculated at each point in the AFM indentation using Hertz and Dimitriadis models is shown for an aE-48%-*p*N_3Phe film (height 418 nm, same film as Figure 5.3). The height-dependent Dimitriadis model gives a consistent modulus in the > 15 nm range, while the Hertz model overestimates E and is indentation-dependent. Distortions caused by applying the Hertz model increase rapidly for thinner films.

A single value of Young's modulus (E) was assigned to each surface by averaging the model-predicted moduli from 15 nm to 10% strain; the standard deviation in E over this range averaged 3.4% and was <10% for all curves, indicating that the Dimitriadis model gives uniform predictions of E. In general, the model-calculated value of E is sensitive to the placement of the contact point,[29] but since contact is observed directly and the sub-15 nm data are excluded, the fits are robust. Illustrations of the fit of the Dimitriadis model to the experimental AFM data are shown in Figure 5.6.

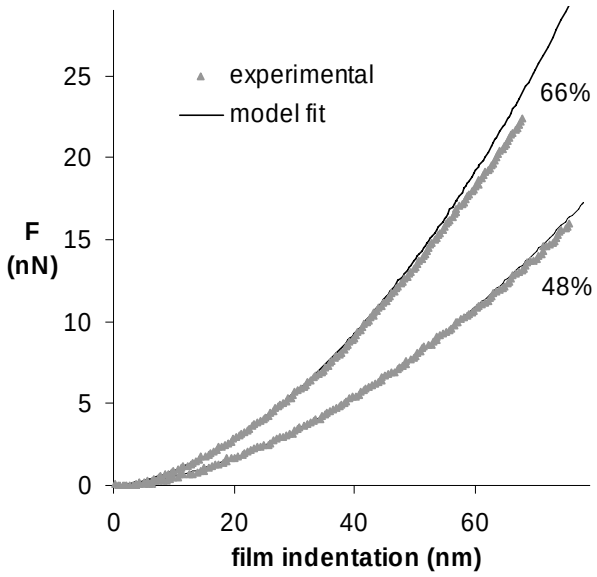

Figure 5.6 Experimental AFM indentation data compared to Dimitriadis model fits for thin films of aE-66%-*p*N_3Phe and aE-48%-*p*N_3Phe (same as in Figures 5.3 & 5.5). To constrain the analysis to the linear elastic range, the model was fit to data between 15 nm and 10% of the film height (33 nm for aE-66%-*p*N_3Phe, 42 nm for aE-48%-*p*N_3Phe), although it fits the experimental data at higher extensions nearly as well, owing to the elasticity of the protein.

Standard deviation in *E* from repeated indentation of the same spot (n=3-4 indents, 51 spots) averaged 5.1%. There was no tendency of the film to become more or less stiff with repeated indentation. Standard deviation in *E* between different spots on the same film (n=3-4 spots, ≥10 μm apart, 13 films) averaged 7.2%, nearly as small as the same-spot variance, indicating that *E* was uniform over the films. The uniformity of modulus is important for the application of these films as probes of mechanosensitive cell behavior.

In principle, raw AFM data could be used to estimate a film thickness, by iterating the height parameter in equation (2) to minimize the variation in

predicted modulus over the selected strain range, since over- or underestimated thickness will result in less consistent modulus predictions. For this technique to be applied, the linear model would need to completely describe the material mechanics in the analyzed strain range. However, experimental error makes it likely that decreases in film thickness could be mistaken for increases in stiffness, or vice-versa. The determination of modulus is more accurate when the exact film thickness is known, as it is here.

5.4.4 Finite element simulation of indentation.

All bulk tensile data were well-described by a Yeoh hyperelastic model.[34] When the Yeoh parameters calculated from the tensile data (*vide infra; see Figure 5.8*) were used to model indentation using a finite element simulation, the predicted force curves were very similar to those obtained experimentally; representative data are presented in Figure 5.7. Because of the experimental error in measuring quantities like the bulk film thickness or AFM cantilever spring constant, some differences in scalar magnitude between these two plots can be expected, although their shapes should be similar, as is seen here. The similarity between experimental AFM indentation data and simulations of the indentation using only bulk tensile properties is encouraging since it implies that the physical properties of thin and bulk films are similar, and it confirms the physical validity of the finite element analysis technique.

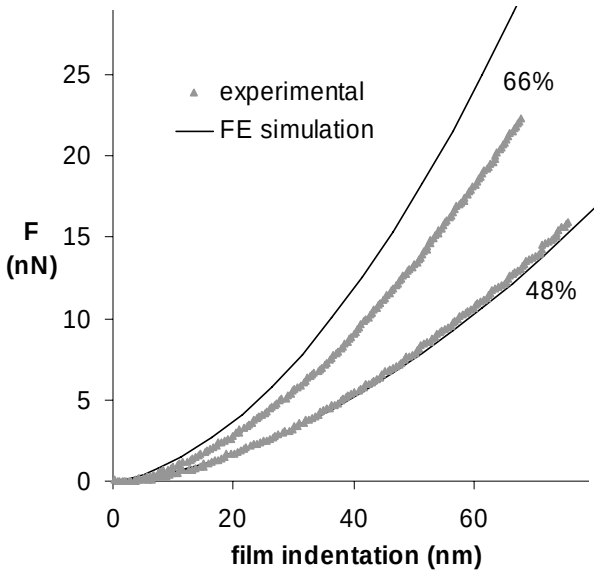

Figure 5.7 Superposition of experimental AFM data (from Figure 5.6) and finite element simulations of indentation based on bulk tensile data for protein films of aE-66%-*p*N_3Phe and aE-48%-*p*N_3Phe.

The samples investigated here are thick relative to the indentation depth and are highly elastic, so the deviations from linearity are small, as can be seen by comparing the linear model fit with experimental AFM data in Figure 5.6. However, the simulation approach should be applicable to thinner films (e.g., <100 nm) and to non-linear strain data as well, where a limited amount of data can be collected in the linear deformation range. While the Dimitriadis model is restricted to spherical tips, the simulation can be easily changed to describe conical or pyramidal tips, the type more commonly used because of their robustness and lower cost. These sharp tips have the additional advantage of being usable for imaging as well as indentation.

Inverting the technique of predicting the AFM response from the tensile data, the AFM data was used to calculate a modulus for the material using the

simulation. To accomplish this, coefficients of the Yeoh model were iterated in the finite element simulation to minimize the difference between the simulated and experimental AFM data using the entire force curve (including data past 10% indentation). The calculated *E* using this technique were indistinguishable from the *E* calculated with the Dimitriadis model. If high-strain data are collected, this technique can provide a full strain function for the material being tested in addition to the elastic modulus. While the finite element technique provides more flexibility, the simplicity of the Dimitriadis model is preferable when the geometry of the tip is known and when the linear elastic modulus *E* is the only value required.

5.4.5 Modulus control by variable incorporation of p*N*$_3$*Phe – bulk films.*

The incorporation of *p*N$_3$Phe in place of Phe in the artificial extracellular matrix protein can be tuned by varying its concentration during bacterial fermentation.[22] Here, the effects of the variable incorporation are shown for both bulk samples tested in uniaxial tension and thin-film samples tested with AFM nanoindentation. The tensile behavior of the bulk samples, in Figure 5.8 below, is typical of rubbery materials, and all aE-*p*N$_3$Phe films were extensible to 150% strain or greater.

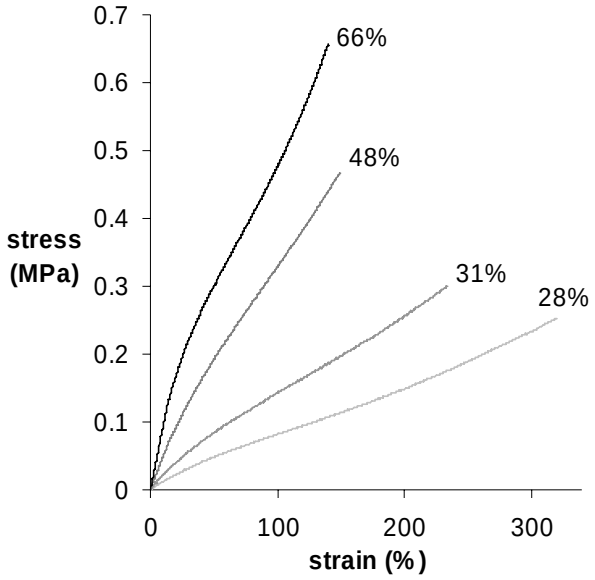

Figure 5.8 Sample tensile data for bulk films of aE-*p*N$_3$Phe, where the replacement of *p*N$_3$Phe for Phe was 28%, 31%, 48%, and 66%.

Higher moduli are seen for films made from protein with higher *p*N$_3$Phe concentrations, a result of increased crosslink densities after irradiation. If the materials are assumed to behave as ideal rubber networks, an approximation shown to be roughly valid for similar elastin-like hydrogels,[15,33] $G=(\rho RT/M_c)(1-2M_c/M)$.[35] G is the shear modulus, equal to one third the elastic modulus *E* for an incompressible material ($\nu=0.5$), a good approximation for the rubbery hydrogel protein films. The chain mass density ρ is found by multiplying the density of elastin,[36] 1.32 g/cm^3, by the measured polymer volume fraction in the films, 0.56. RT, the absolute temperature, is 22 °C = 2454 J/°K/mol. M_c is the average molecular weight between crosslinks, and the term $(1-2M_c/M)$ represents the fraction of elastically active crosslinks, where M is the molecular weight of the protein, 42.9 kDa. The M_c calculated for these films are listed in Table 5.1 A.

Table 5.1 (A) Physical properties of bulk aE-*p*N$_3$Phe films tested in uniaxial tension (n=2). (B) Physical properties of thin aE-*p*N$_3$Phe films tested by AFM (n≥6 spots, n≥24 total indents). The elastic moduli are indicated graphically in Figure 5.9.

A bulk

protein	thickness (μm)	avg. elastic modulus *E* (MPa)	mol. wt. between crosslinks M_c (kDa)	reaction efficiency
aE-66%-*p*N$_3$Phe	20	1.01 ± 0.07	4.3 ± 0.2	50 ± 3%
aE-48%-*p*N$_3$Phe	21	0.52 ± 0.04	7.0 ± 0.4	42 ± 2%
aE-31%-*p*N$_3$Phe	19	0.20 ± 0.04	11.9 ± 1.0	39 ± 3%
aE-28%-*p*N$_3$Phe	20	0.14 ± 0.02	13.8 ± 0.6	37 ± 2%

B AFM

protein	avg. thicknesses (nm)	avg. elastic modulus *E* (MPa)	mol. wt. between crosslinks M_c (kDa)	reaction efficiency
aE-66%-*p*N$_3$Phe	312, 322, 328, 1682, 1466	0.91 ± 0.16	4.9 ± 0.7	45 ± 7%
aE-48%-*p*N$_3$Phe	293, 368	0.44 ± 0.04	7.8 ± 0.4	38 ± 2%
aE-31%-*p*N$_3$Phe	223, 252	0.30 ± 0.02	9.8 ± 0.4	47 ± 2%
aE-28%-*p*N$_3$Phe	206, 206	0.29 ± 0.03	10.0 ± 0.5	51 ± 3%

Using M_c and the measured *p*N$_3$Phe incorporation, a crosslinking reaction efficiency can be calculated. For example, M_c = 4.3 kDa for aE-66%-*p*N$_3$Phe corresponds to 42.9/4.3 = 10 crosslinks per protein molecule, assuming random crosslinking, which is reasonable given the periodic Phe spacing in the protein and the statistical nature of its replacement by *p*N$_3$Phe. A 66% replacement of the 15 Phe sites in aE implies an average of 9.9 *p*N$_3$Phe side chains per molecule;

since each insertion crosslinks two molecules, this implies a reaction efficiency of 10/9.9/2 = 50%. The other films suggest efficiencies of 37-42% (Table 5.1 A). The efficiencies may be overestimated somewhat because entanglements may serve as additional effective crosslinks. In any case, the efficiency of photocrosslinking is high; the density of the protein phase (dry films) during photocrosslinking is likely one reason.

5.4.6 Modulus control by variable incorporation of pN_3*Phe – thin films.*

Figure 5.9 compares the elastic moduli, *E*, calculated from AFM data for thin films of variable *p*N_3Phe concentration to the values from uniaxial tension. For aE-48%-*p*N_3Phe and aE-66%-*p*N_3Phe, the values match within experimental error, indicating that the mechanical properties of the bulk films can be reproduced in films 200-400 nm thick, and supporting the validity of the Dimitriadis model for measuring *E*. The bulk and thin films, although cast from different solvents, are both crosslinked in the dry state, and are thus expected to have similar structures and elastic moduli.

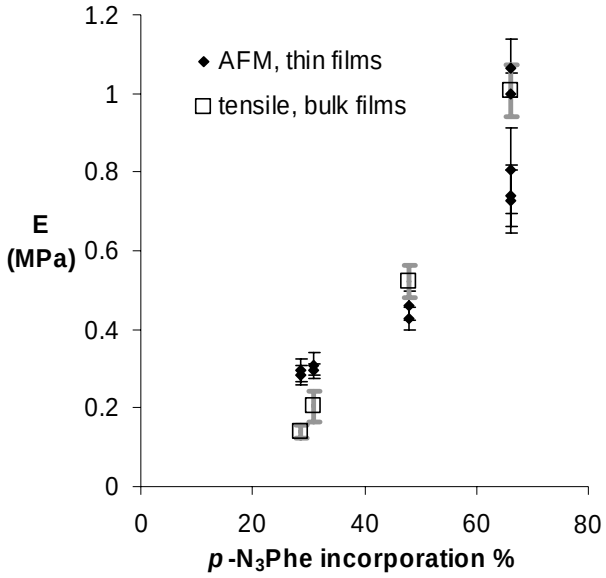

Figure 5.9 Measured elastic moduli of thin films of aE-*p*N3Phe versus fraction replacement of *p*N3Phe for Phe. Results from AFM nanoindentation of thin films and tensile testing of bulk films are compared. Separate data points are plotted for each film tested by AFM, with error bars indicating the standard deviation in *E* in a given film (n≥3 spots; n≥11 total indents). Standard deviation for tensile samples are also shown (n=2).

At low pN3Phe incorporation levels, the AFM seems to have yielded moduli slightly higher than those obtained from the tensile measurements; it is unclear whether this is due to unaccounted-for experimental error or some other factor. The analysis of reaction performed on the bulk films was repeated using the thin film moduli, and the resulting efficiencies were between 38 and 51% (Table 5.1 B).

The ability to tune the modulus of the thin films by variable *p*N3Phe incorporation should prove useful in cell-culture experiments designed to study mechanosensitive cell behavior on materials with coordinating biological signals

like the CS5 domain in protein aE. Cell behavior can be compared on substrates with systematic variations in modulus, although for certain studies, patterns of stiffness on a single film may be preferred. For example, a microfluidic mixer[13,37] may allow gradient formation from these proteins. aE-*p*N_3Phe with high and low *p*N_3Phe incorporation levels could be introduced to either side of a gradient generator and uniformly crosslinked once deposited on a surface.

5.4.7 Modulus control by variable irradiation of p*N₃Phe*

Controlling mechanical properties by differential irradiation allows films with patterns of stiffness to be made. A film containing a step gradient of stiffness was created here by UV-irradiating successive portions of the same film, made from aE-66%-*p*N_3Phe, for increasing lengths of time. The calculated elastic modulus, *E*, versus irradiation is shown in Figure 5.10 below; a greater-than-twofold variation in modulus is seen between 20 sec and 300 sec irradiation. The majority of the rise in stiffness occurs over the first minute of UV exposure, with a gradual plateau thereafter. The time required for *p*N_3Phe depletion is similar to that reported previously under similar irradiation conditions.[22]

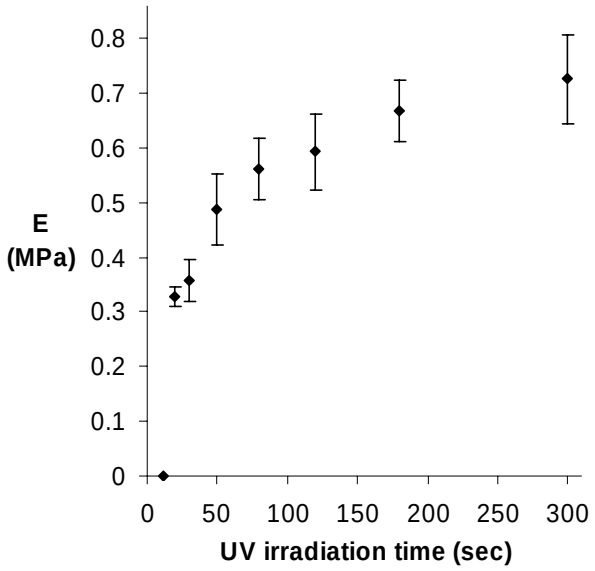

Figure 5.10 Modulus variation by variable irradiation on a single aE-66%-*p*N$_3$Phe film. Error bars indicate standard deviation in *E* within each zone of the step-gradient (n≥3 spots, n≥8 total indents per zone). Irradiation for 12 sec was not sufficient to form a crosslinked network, i.e., $E = 0$.

When washed to remove soluble protein, the thicknesses of the 20 sec and 30 sec zones along the gradient were ~35% and ~20% less than the thickness of the 80 sec and greater zones, indicating partial solubility. Taking into account the known film height, as the Dimitriadis model does, is essential for these gradients, since variable film height would make the Hertz model inaccurate even as a comparative measure of modulus.

Individual films that vary spatially in modulus on millimeter length scales, as in the step-gradient pattern created here, are useful in characterizing cell behavior. Large numbers of cells can be cultured on each zone, allowing average cell properties to be measured on several stiffness zones on a single substrate, which minimizes reagent usage and substrate preparation, and avoids

batch-to-batch variations in films and cells. Additionally, the ability to observe cell behavior at mechanical interfaces can be quite valuable on its own.[5] Films with more complex patterns of mechanical properties can also be envisioned. UV photoirradiation through a mask, which has already been used to pattern proteins into defined locations on a support,[22] could be applied to creating films with micropatterned moduli; cell behavior on micropatterned materials has been the subject of considerable recent study.[38]

While step gradients are easy to characterize with a limited number of indentations, films with continuous gradients of stiffness could also be made with the variable irradiation approach by moving an opaque shutter across the film during irradiation.[39] Gradients could be implemented over either short or long distances in the film. For steep gradients, the spatial resolution of the modulus measurement is limited only by the 300 nm-radius tip used for indentation, which should enable measurement of the variation in mechanical properties under a single spread cell. Even higher resolution may be achieved through use of conventional sharp (<20 nm) conical or pyramidal tips with finite element analysis of indentation. Gradients longer than the ~100 μm lateral piezo range of conventional AFM instruments could be characterized using translational reference points in the sample. The characterization would be facilitated by an automated technique to indent and analyze an array of spots on a sample.

5.5 Conclusions

The ability to incorporate the photosensitive amino acid *para*-azidophenylalanine into artificial proteins has made it possible to create mechanically variant thin protein films. A film height-dependent indentation model, whose results were confirmed by bulk tensile data and finite element simulation, allowed the moduli of the films to be confidently measured. These thin films are intended for use as substrates to characterize mechanosensitive cell behavior in the context of coincident biological signals. The results provide methods for making individual films with complex variations in stiffness, such as patterns and gradients, and the resolution and flexibility of the AFM technique used here should make characterizing their stiffness straightforward.

While the existing protein can be used to probe cell interactions with the CS5 binding domain, the platform for making photosensitive artificial proteins can be extended to other peptide domains of interest; we are currently characterizing RGD-containing photosensitive protein films. A better understanding of cell response to coordinating biological and mechanical signals will aid the design of functional biomaterials.

Acknowledgements

Stacey Maskarinec made proteins aE-28%-*p*N_3Phe, aE-31%-*p*N_3Phe, and aE-66%-*p*N_3Phe. Marissa Mock performed the NMR characterizations. Funding was provided by the NSF MRSEC Center for the Science and Engineering of Materials at Caltech, and by the NIH (HL 59987).

5.6 References

(1) Pelham RJ, Wang YL. Cell locomotion and focal adhesions are regulated by substrate flexibility. *Proc. Natl. Acad. Sci. U. S. A.* **1997**, *94*, 13661-13665.

(2) Cukierman E, Pankov R, Stevens DR, Yamada KM. Taking cell-matrix adhesions to the third dimension. *Science* **2001**, *294*, 1708-1712.

(3) Engler A, Bacakova L, Newman C, Hategan A, Griffin M, Discher D. Substrate compliance versus ligand density in cell on gel responses. *Biophys. J.* **2004**, *86*, 617-628.

(4) Engler AJ, Richert L, Wong JY, Picart C, Discher DE. Surface probe measurements of the elasticity of sectioned tissue, thin gels and polyelectrolyte multilayer films: Correlations between substrate stiffness and cell adhesion. *Surf. Sci.* **2004**, *570*, 142-154.

(5) Lo CM, Wang HB, Dembo M, Wang YL. Cell movement is guided by the rigidity of the substrate. *Biophys. J.* **2000**, *79*, 144-152.

(6) Gray DS, Tien J, Chen CS. Repositioning of cells by mechanotaxis on surfaces with micropatterned Young's modulus. *J. Biomed. Mater. Res. A* **2003**, *66A*, 605-614.

(7) Wang HB, Dembo M, Wang YL. Substrate flexibility regulates growth and apoptosis of normal but not transformed cells. *Am. J. Physiol. - Cell Ph.* **2000**, *279*, C1345-C1350.

(8) Engler AJ, Griffin MA, Sen S, Bonnetnann CG, Sweeney HL, Discher DE. Myotubes differentiate optimally on substrates with tissue-like stiffness: pathological implications for soft or stiff microenvironments. *J. Cell Biol.* **2004**, *166*, 877-887.

(9) Discher DE, Janmey P, Wang YL. Tissue cells feel and respond to the stiffness of their substrate. *Science* **2005**, *310*, 1139-1143.

(10) Wang YL, Pelham RJ In *Molecular Motors and the Cytoskeleton, Pt B*, **1998**; Vol. 298, pp 489-496.

(11) Maskarinec SA, Tirrell DA. Protein engineering approaches to biomaterials design. *Curr. Opin. Biotechnol.* **2005**, *16*, 422-426.

(12) Wong JY, Velasco A, Rajagopalan P, Pham Q. Directed movement of vascular smooth muscle cells on gradient-compliant hydrogels. *Langmuir* **2003**, *19*, 1908-1913.

(13) Zaari N, Rajagopalan P, Kim SK, Engler AJ, Wong JY. Photopolymerization in microfluidic gradient generators: Microscale control of substrate compliance to manipulate cell response. *Adv. Mater.* **2004**, *16*, 2133-2137.

(14) Panitch A, Yamaoka T, Fournier MJ, Mason TL, Tirrell DA. Design and biosynthesis of elastin-like artificial extracellular matrix proteins containing periodically spaced fibronectin CS5 domains. *Macromolecules* **1999**, *32*, 1701-1703.

(15) Welsh ER, Tirrell DA. Engineering the extracellular matrix: A novel approach to polymeric biomaterials. I. Control of the physical properties of artificial protein matrices designed to support adhesion of vascular endothelial cells. *Biomacromolecules* **2000**, *1*, 23-30.

(16) Di Zio K, Tirrell DA. Mechanical properties of artificial protein matrices engineered for control of cell and tissue behavior. *Macromolecules* **2003**, *36*, 1553-1558.

(17) Liu JC, Heilshorn SC, Tirrell DA. Comparative cell response to artificial extracellular matrix proteins containing the RGD and CS5 cell-binding domains. *Biomacromolecules* **2004**, *5*, 497-504.

(18) Mould AP, Komoriya A, Yamada KM, Humphries MJ. The CS5 Peptide Is a 2nd Site in the IIICS region of fibronectin recognized by the integrin alpha-4-beta-1 - inhibition of alpha-4-beta-1 function by RGD peptide homologs. *J. Biol. Chem.* **1991**, *266*, 3579-3585.

(19) Urry DW. Physical chemistry of biological free energy transduction as demonstrated by elastic protein-based polymers. *J. Phys. Chem. B* **1997**, *101*, 11007-11028.

(20) Kast P, Hennecke H. Amino-acid substrate-specificity of escherichia-coli phenylalanyl-transfer RNA-synthetase altered by distinct mutations. *J. Mol. Biol.* **1991**, *222*, 99-124.

(21) Kirshenbaum K, Carrico IS, Tirrell DA. Biosynthesis of proteins incorporating a versatile set of phenylalanine analogues. *Chembiochem* **2002**, *3*, 235-237.

(22) (Appendix) Carrico IS, Heilshorn SC, Mock ML, Liu JC, Nowatzki PJ, Maskarinec SA, Franck C, Ravichandran G, Tirrell DA. Lithographic patterning of intrinsically photoreactive cell-adhesive proteins. *Prepared for submission.*

(23) Vinckier A, Semenza G. Measuring elasticity of biological materials by atomic force microscopy. *FEBS Lett.* **1998**, *430*, 12-16.

(24) Cappella B, Dietler G. Force-distance curves by atomic force microscopy. *Surface Science Reports* **1999**, *34*, 1-103.

(25) Heinz WF, Hoh JH. Spatially resolved force spectroscopy of biological surfaces using the atomic force microscope. *Trends Biotechnol.* **1999**, *17*, 143-150.

(26) Mahaffy RE, Shih CK, MacKintosh FC, Kas J. Scanning probe-based frequency-dependent microrheology of polymer gels and biological cells. *Phys. Rev. Lett.* **2000**, *85*, 880-883.

(27) Richert L, Engler AJ, Discher DE, Picart C. Elasticity of native and cross-linked polyelectrolyte multilayer films. *Biomacromolecules* **2004**, *5*, 1908-1916.

(28) Costa KD, Yin FCP. Analysis of indentation: Implications for measuring mechanical properties with atomic force microscopy. *J. Biomech. Eng.* **1999**, *121*, 462-471.

(29) Dimitriadis EK, Horkay F, Maresca J, Kachar B, Chadwick RS. Determination of elastic moduli of thin layers of soft material using the atomic force microscope. *Biophys. J.* **2002**, *82*, 2798-2810.

(30) Domke J, Radmacher M. Measuring the elastic properties of thin polymer films with the atomic force microscope. *Langmuir* **1998**, *14*, 3320-3325.

(31) Akhremitchev BB, Walker GC. Finite sample thickness effects on elasticity determination using atomic force microscopy. *Langmuir* **1999**, *15*, 5630-5634.

(32) Sharma N "Biosynthetic introduction of aryl bromide functionality into proteins," Ph.D. Thesis, University of Massachusetts Amherst, **2001**.

(33) Nowatzki PJ, Tirrell DA. Physical properties of artificial extracellular matrix protein films prepared by isocyanate crosslinking. *Biomaterials* **2004**, *25*, 1261-1267.

(34) Yeoh OH. Some forms of the strain-energy function for rubber. *Rubber Chem. Technol.* **1993**, *66*, 754-771.

(35) Flory PJ. *Principles of Polymer Chemistry*; Cornell University Press: Ithaca, NY, **1953**.

(36) Lillie MA, Gosline JM. Unusual swelling of elastin. *Biopolymers* **2002**, *64*, 115-126.

(37) Jeon NL, Dertinger SKW, Chiu DT, Choi IS, Stroock AD, Whitesides GM. Generation of solution and surface gradients using microfluidic systems. *Langmuir* **2000**, *16*, 8311-8316.

(38) Stevens MM, George JH. Exploring and engineering the cell surface interface. *Science* **2005**, *310*, 1135-1138.

(39) Pucci V, Raggi MA, Svec F, Frechet JMJ. Monolithic columns with a gradient of functionalities prepared via photoinitiated grafting for separations using capillary electrochromatography. *J. Sep. Sci.* **2004**, *27*, 779-788.